Studying Hadronic Reactions: K_L Beam Production of Ξ^- Hyperons on a Deuterium Target

Maya Jovanović

Department of Physics

May 2022

This report explores the feasibility of commencing the experimental scattering of Ξ^- hyperons with protons in a deuterium target at the Thomas Jefferson Laboratory. This experiment intends to provide uniquely obtained measurements which will subsequently support the study of hyperon-nucleon interactions and their role in high-density environments such as neutron stars, ultimately paving a path to solving the “Hyperon Puzzle”. The feasibility of this experiment is determined following the results of a Monte-Carlo simulation of the proposed $K_L + n \rightarrow K^+ + \Xi^-$ production interaction using the ROOT computational framework. Results from the completed simulation run produce a detected scattered Ξ^- yield of ~700 hyperons. Conclusively, it is recommended that running the experiment is feasible, since the obtained statistics are much higher than those previously measured.

Contents

1. Introduction

Hyperons are highly unstable baryons containing one or more strange quarks, and are hypothesised to exist in a stable form in extremely gravitationally massive and dense environments - such as the core of a neutron star [1]. As a consequence, the equation of state (EoS) does not apply to neutron stars, unlike with other typical stars with a much smaller gravity and density. Thus, the existence of hyperons in such environments is considered unavoidable, yet this is contradictory with previously measured masses of neutron stars as their existence would imply a discrepancy in the maximum mass permitted [2]. This discrepancy as well as that in the EoS due to the existence of hyperons is detailed in Figure 1, and is often referred to as the "Hyperon Puzzle". This "softening" of the EoS implies that hyperons cause the canonical mass of neutron stars to be significantly lower than measured.

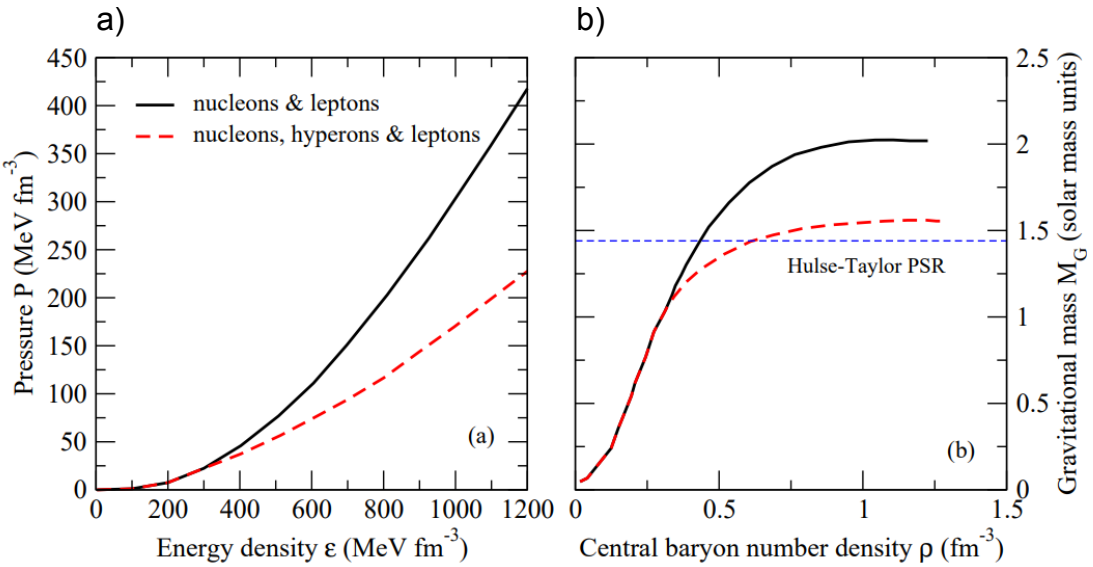

Figure 1: A generic model with (black solid line) and without (red dashed line) hyperons has been considered. The horizontal line shows the observational mass of the Hulse–Taylor pulsar [4]. a) Effect of hyperons on the EoS. b) Effect on neutron star mass. Figure from reference [3].

Some of the most important known hyperon-nucleon interactions within a neutron star are those involving the cascade baryon, Ξ^-. The name "cascade" originates from its multi-step decay process: it most commonly decays to a Λ^0 hyperon and π^-, and Λ^0 subsequently decays into a proton-π^- pair [5]. Yet, due to a lack of substantial knowledge about their interactions with matter within them, the complete role that hyperons play in neutron stars is still unclear. Hence, there is a strong incentive to continue studies into hyperonic behaviour - recent gravitational wave observations of neutron stars [6] imply that gathering experimental measurements of hyperon-nucleon interactions would be especially relevant to further our understanding of this phenomenon. To address such matters, a hyperon beam facility is currently being constructed in the Thomas Jefferson labs (JLab), where the Kaon-Long Facility (KLF) Collaboration is modifying the existing GlueX detector in Hall D [7].

1.1 Project Aims and Motivations

The aim of this project is to simulate the scattering events that would occur when a neutral Kaon-long beam, K_L, hits a deuterium target thus producing a positively charged Kaon, K^+, and a negatively charged Ξ^- hyperon. The hyperon would then scatter elastically with protons in the deuterium target. In particle notation, this interaction can be expressed as:

$$K_L + n \rightarrow K^+ + \Xi^- \tag{1}$$

$$\Xi^- + p \rightarrow \Xi^- + p \tag{2}$$

The successful completion of this proposed experiment would provide the first ever recorded measurements for neutral kaons incident on such a target [8]. Producing a comprehensive simulation of this scattering event involves writing a macro using the C++ language, and comprehensively utilising ROOT[1] in order to run the code. The aim of the simulation is to explore the feasibility of running the experiment at JLab, by evaluating the expected statistics of the produced cascades and their scattering events, and the probability that their final decay state is measured within the GlueX detector acceptance, where the acceptance calculations account for the parameters of the detector. An accurately computed simulation will allow for the prediction of the number of events that would occur. The data is to be generated with random values using the Monte-Carlo method, and the outcome will ultimately determine whether conducting the experiment with the modified particle detector in Hall D is feasible.

Preliminary studies are necessary for research into these undocumented interactions due to the high cost of running the experiment at JLab. Thus far, the GlueX detector produced excellent results with a photon beam for the production of hybrid mesons, [9] and so there is a compelling motivation for the exploration of hyperonic reactions using such equipment. A successful run of the experiment would ultimately lead to a new insight into the accuracy of quantum chromodynamics of hyperons, as well enabling precise partial-wave analysis of resonances in the spectra of a variety of hyperons [10].

2. Methods

The component analysis of the computational and mathematical concepts in Sections 2.1 and 2.2 are necessary in order to build a foundation for the program. The two components must be combined in order to finalise an accurate method for gathering the data required for this feasibility study. Ensuring that the mathematics is correct is paramount to the obtaining of realistic results.

[1] ROOT is a framework for data processing made by CERN. See Ref [11].

2.1 Programming

The Monte-Carlo (MC) method, used primarily in computational algorithms, is when events are simulated, repetitively, by values obtained via random sampling as dictated by a program macro. The values obtained via this random sampling are drawn from a probability distribution. For interactions within a multi-dimensional frame, such as a particle interaction, MC methods can be especially useful, due to the number of coupled degrees of freedom that need to be accounted for. As such, MC simulations may be considered as a test for a program - whether it will produce consistent data regardless of the amount of times the simulation has been run.

For this project, a more simplistic approach to MC simulations is taken, by using the ROOT framework. The initial creation of ROOT was for use in high energy physics data analysis for various CERN projects [11]. It is written in and designed to be used with the C++ programming language due to its designation as an object-oriented program, though it supports the use of other languages. ROOT also has a wide range of classes available in its extensive library, making it ideal for high-performance computing and data mining [12]. C++ is a general purpose language designed for many uses due to it being cross-platform accessible, and has great flexibility in computational ability and application. For this computational project, there was optionality of choice for which release of ROOT to use. The ROOT 5.34/38 release allows for two different types of syntax, whereas the most recent releases of ROOT (6.0 onwards) are more limited in this regard.

The simulation is to be run for a user-defined number of events, typically a number above 100,000 in order to obtain more conclusive results with a much smaller margin of error. For each event simulated, an interaction phase space will be generated, where each stage of the particle interaction is designated as a “vertex”. These vertices require their own phase spaces due to the momentum and mass four-vectors differing in each vertex. Thus, what can be considered as the first stage of MC-style simulating takes place once all variables have been defined in the code.

2.2 Mathematical Concepts

Analysing a scattering problem by splitting it up into its constituent angular momentum components is called partial-wave analysis (PWA), but whilst that is the general mathematical concept in application, it is not the focus of this project. Nonetheless, it is useful to note in order to justify the methods used while executing the program, and that constraining the PWAs of hyperon scattering, thus reducing uncertainties in the model calculation, is one of the consequences of running the experiment at JLab [7]. There are three key elements of the fundamental mathematics of the interaction - the production cross section, the luminosity, and the length of the path the particle travels within the target.

2.2.1 Cross Section and Luminosity

For the liquid deuterium[2] target of density ρ_d and length L_t, with a flux F_{Kl} of beam particles incident onto it, the luminosity of the beam (denoted as λ) is defined as:

[2] The density of liquid deuterium is 0.0001624 kg cm^{-3}.

$$\lambda = F_{Kl}\rho_d L_t \tag{3}$$

When the luminosity is multiplied by the production cross section, σ, of the interaction, the resultant product is the number of interaction events per second of that particle production, $\frac{dN}{dt}$. This is essentially another way of describing the flux of particle events [13]. The number of Ξ^- produced per second in the target is shown in Equation 4, where σ_{Kl} is the production cross section of the K_L beam interaction.

$$\frac{dN(\Xi)}{dt} = \lambda\sigma_{Kl} \tag{4}$$

Luminosity is also used to calculate the length of the Ξ^- trajectory. Using Equation 3, the length L_t can be substituted for this path length, and the number of production events $\frac{dN}{dt}$ becomes the new flux, F_{Ξ}, in place of F.

$$\lambda = F_{\Xi}\rho_d L_{path} \tag{5}$$

From this, to find the number of Ξ^- particles which get scattered per second in the target, the average cross section of the Ξ^- + p scattering of 5.25 millibarns[3] [14], $\sigma_{\Xi p}$, is used in place of σ_{Kl} in Equation 4. The final number of detected scattering events is determined by integrating the resultant differential equation with respect to time. The integration must be in terms of seconds, not days, in order to preserve the units of calculation. From observing the results, the feasibility of performing the study at JLab can be ascertained. This is dependent on how many data points have been collected.

2.2.2 Path Length

The beam-target interaction had to be considered in two planes of the cylindrical target, as detailed in Figures 2 and 3, in order to determine the true three dimensional calculation of the trajectory magnitude. The target is a cylinder with a length of 40 centimetres and a diameter of 6 centimetres. It contains liquid deuterium. The beam enters the target and hyperon production occurs at the (x, y, z) vertex. The particle produced in this reaction then travels within the target and exits the target at an arbitrary (x',y',z') vertex. There is a possibility that the particle decays prior to exiting the target, in which case the (x',y',z') vertex would be the point at which the hyperon decays after travelling some distance.

Figure 2 shows the cylinder when being observed in the two-dimensional (x, y) plane. The third dimension, characterised by the diagonally drawn z axis purely for visual purposes, is going directly orthogonally into the (x, y) plane. The aim is to calculate the length of L, shown as the red solid line. The cosine rule is applied to the

[3] 1 barn = 10^{-24} cm^2.

triangle formed of the various radii within the target, including the radius of the target R, and the formula is rearranged to calculate L [A2.1].

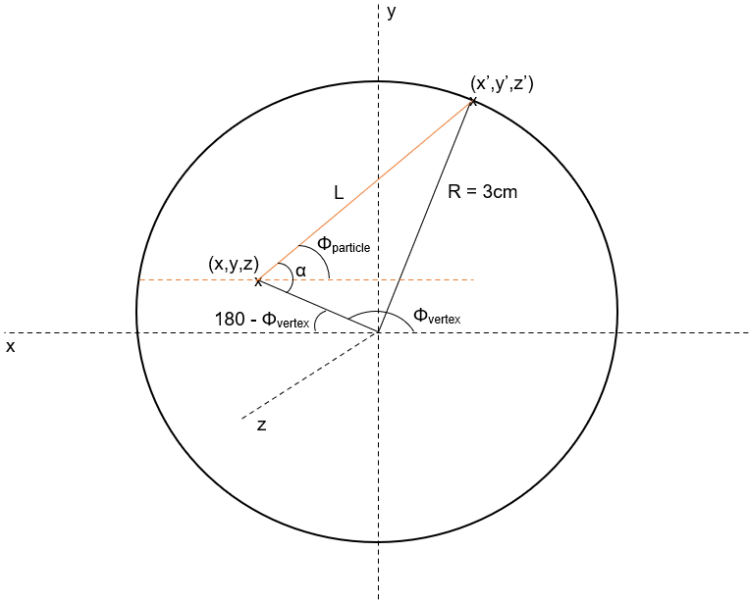

Figure 2: A view of the target cylinder in the (x, y) plane.

Figure 3 presents a more complex planar view. Although one would assume that the "side view" of the target would be the (y, z) plane, one must consider that the length L', shown as the red solid line, cannot be accurately measured along the y axis. It is not representative of its true length due to the three-dimensional perception of it - it would be dilated in the (y,z) plane. Thus, the y axis is more accurately the y-component axis, denoted as ȳ, to which L' is accurately parallel to.

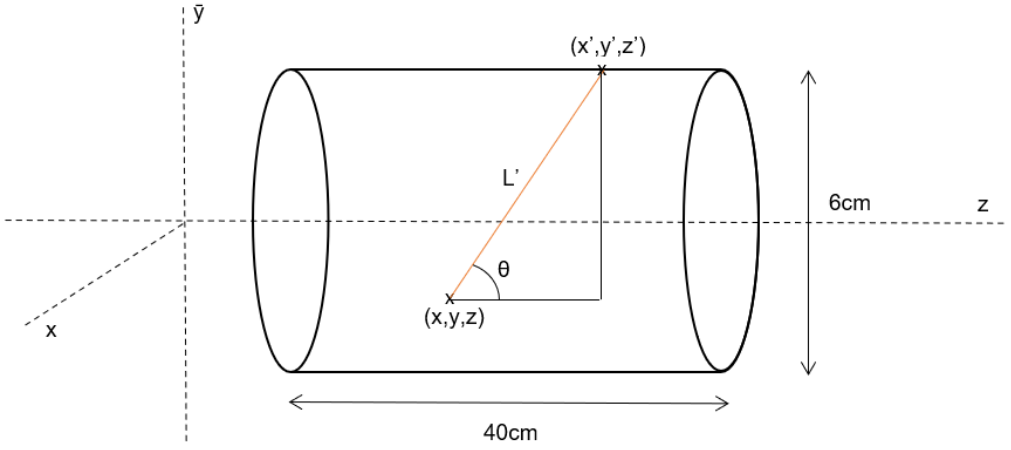

Figure 3: A view of the target cylinder in the (ȳ, z) plane.

If the particle were to exit from the top or bottom of the cylindrical target, the length L' is calculated directly. If z' is either larger than the target length, or smaller than 0, it is assumed that the particle exited from the end caps of the target. For these conditions the complete path length, denoted as L_p, can be directly calculated as shown in Equation 6. However, if the particle scatters and exits at a vertex within the target length, the complete path length can be directly calculated as shown in Equation 7.

$$L_p = \frac{L'}{cos(\theta)} \tag{6}$$

$$L_p = \frac{L}{sin(\theta)} \tag{7}$$

The decay of the particle influences the total path length. Using the finalised path length calculations, the decay length is obtained by combining the exponential decay of the Ξ^- hyperon with a random value generator, and applying it to the randomly simulated data for the path length.

3. Results and Discussion

The full code used to produce these results can be found in Appendix 1. All calculations for values obtained mathematically can be found in Appendix 2. Figures of the additional data plots not shown in this section are available in Appendix 3 onwards.

3.1 Results

3.1.1 Momentum and Cross Sections

Many of the results are dependent on the momentum components of the interaction - for example, the momentum of the cascade hyperon produced when the beam entered the target, and the momentum of the beam prior to entering the target. The flux of the proposed K_L beam at JLab is 10,000 particles per second, and the same value is used for the simulation. However, the beam intensity is not uniform over the energy ranges accessible in the experiment. The beam energy dependence of the K_L beam is sampled from random distributions in order to reproduce the expected intensity [8]. The two plots in Figure 4 are expected to have a similar shape, since the data used to create Figure 4b) is obtained directly from Figure 4a). They are both functions of K_L momentum using a logarithmic scale on the y-axis.

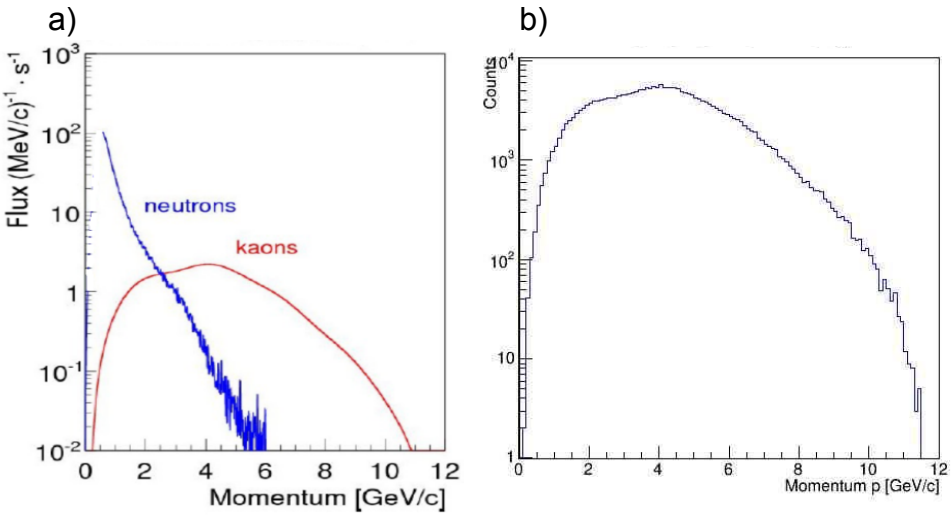

Figure 4: a) Kaon and neutron flux with respect to momentum [8]. b) Momentum of the K_L particles in the beam.

Figure 4a) accounts for the flux of the neutrons after the beam is incident onto the target, and 4b) is a function of the number of counts recorded at specific momenta as the reaction is simulated over 250,000 events.

Due to the undocumented nature of the specific K_L + n interaction being studied in this project, no such cross sectional data exists for a K_L beam incident onto a "neutron" target [8]. Consequently, it was recommended that the cross sectional data available for the $K_L + p \rightarrow K^+ + \Xi^0$ interaction [7] was used, on the assumption that the statistics of the interaction will be similar to that of the undocumented one. This assumption can be made due to the similarity in mass of the particles involved in both interactions. Figure 5 shows a comparison of the interaction parameters plotted by the KLF Collaboration and the cross section histogram used for this project.

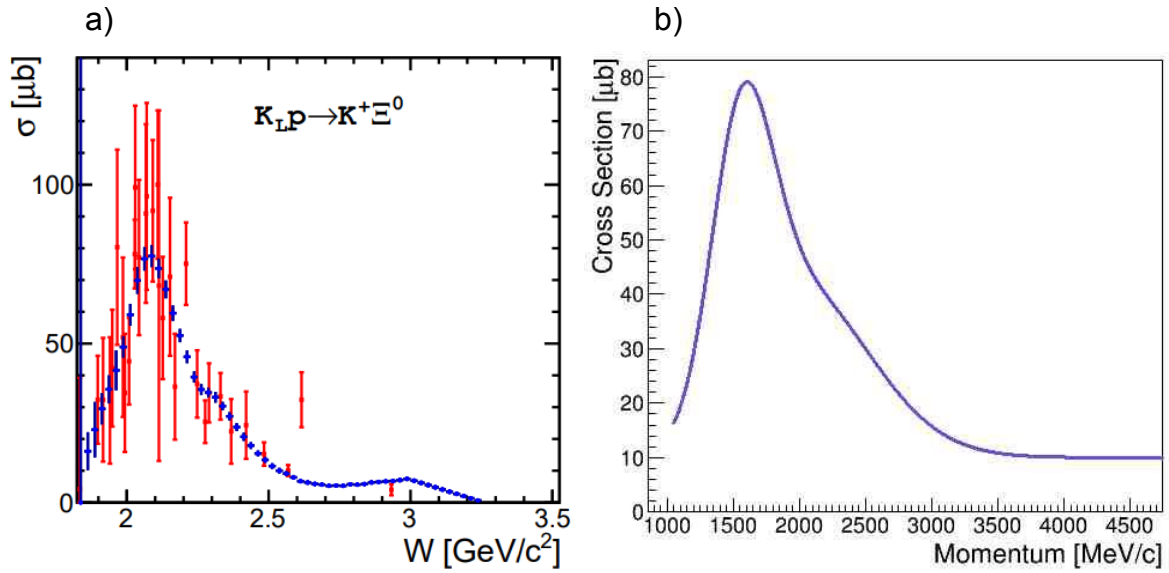

Figure 5: a) The total and differential cross sections with uncertainty estimates, plotted against the invariant mass. Figure from reference [10]. b) The cross section of the $K_Lp \rightarrow K^+\Xi$ interaction, plotted against the momentum.

Both plots have peaks at roughly 2 GeV/c^2 on the left, and 2 GeV/c on the right. The threshold momentum of the K_L beam for the interaction to occur is determined by considering the four-vectors of the interaction particles. At the start of the interaction, the only four-vector with a momentum value is that of the beam. It is known that the beam operates with a K_L momentum of 3.5 GeV/c, which travels along the z-axis as detailed in Figure 3. The minimum beam momentum required for the interaction to occur is calculated as 1.04 GeV/c [A2.2]. This value is supported by the simulated data, aligning with the minimum momentum value recorded as seen in Figure 5b).

The momenta of the initially produced Ξ^- and the rescattered Ξ^-, shown in panels a) and b) of Figure 6 respectively, are calculated within the event loop using a randomly sampled momentum function. Figure 6 shows that the momentum of Ξ^- before it is scattered, which is simulated to peak at about 2 GeV/c, is generally slightly higher than the momentum of around 1 GeV/c after being scattered.

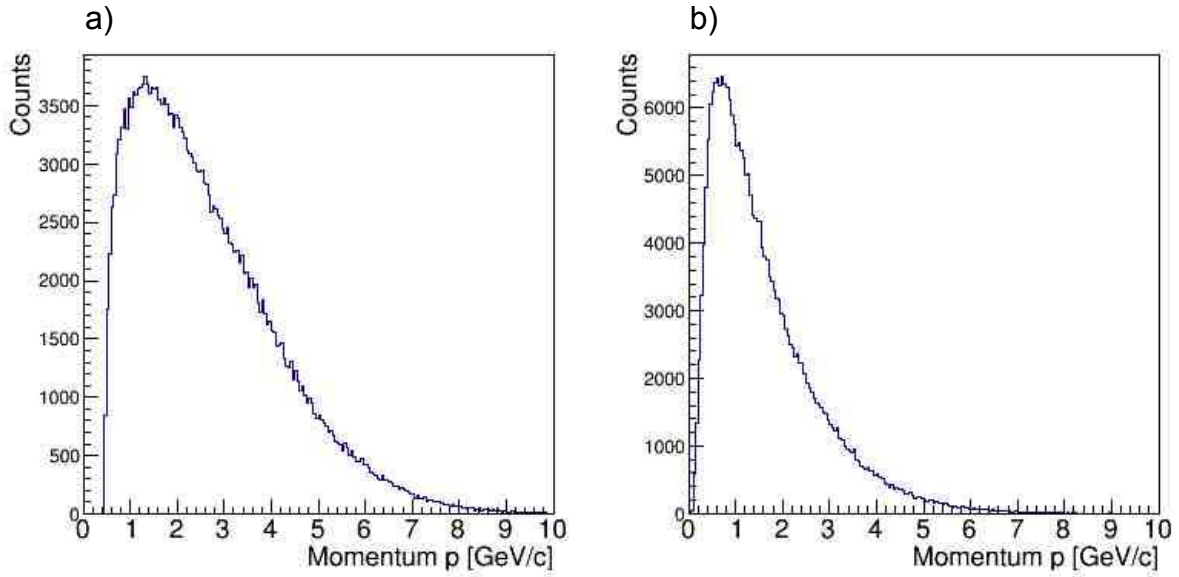

Figure 6: a) Momentum of initially produced Ξ^-. b) Momentum of rescattered Ξ^-.

The conservation of energy and momentum laws apply in all interactions, and in this instance the proton in the scattering vertex carries the remainder of the momentum Ξ^- loses. The steep decrease in momenta on both graphs indicates that less particles are recorded at higher momenta, which could be due to the hyperon taking a longer time to decay or scatter.

3.1.2 Angular Dependence

Figure 7 represents the angles the particles in the initial reaction scatter and rescatter. The regions of concentration in these plots show the frequency of scattering. The colour scale on each histogram represents the density of events per data point. This therefore shows how many particles get scattered at a given angle at each momentum point. For example, Figure 7c) shows that at a momentum of between 0.5 to 1.5 GeV/c, the hyperon is predicted to scatter between the angles of 25 to 60 degrees with a much higher probability.

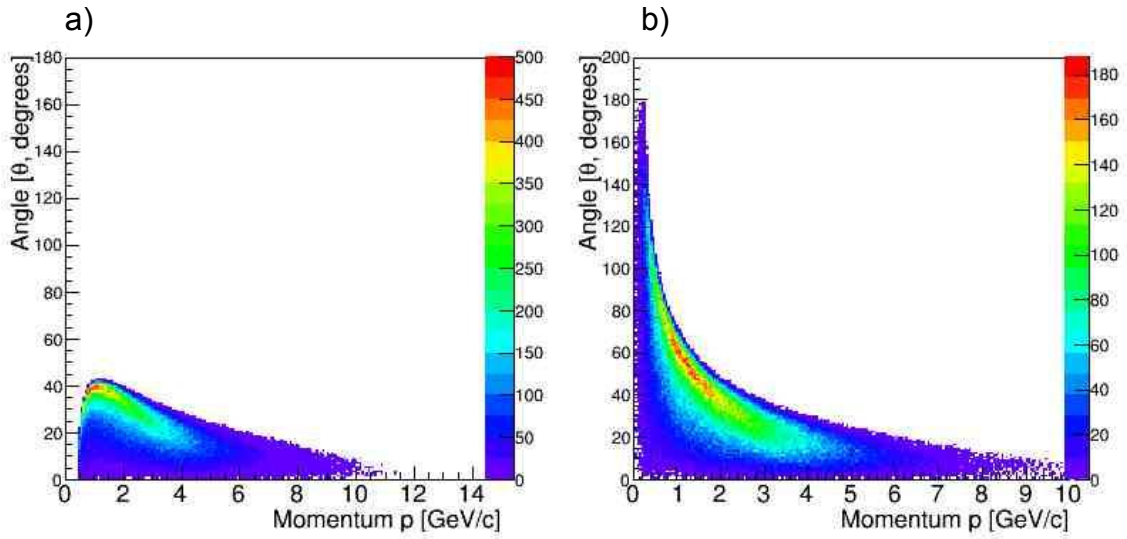

Figure 7: a) Angular dependence of initially produced Ξ^-, b) Angular dependence of K^+.

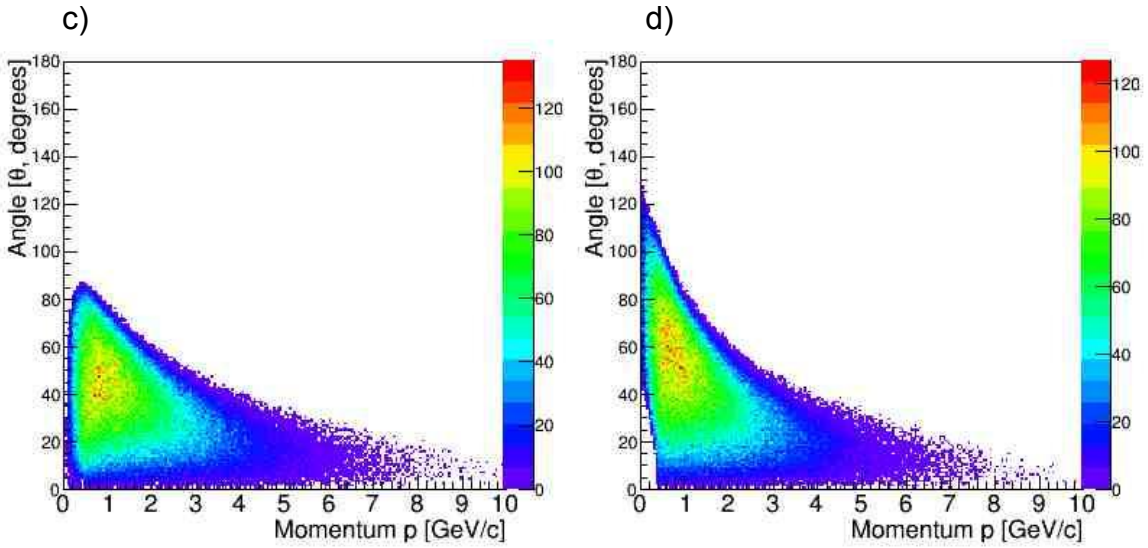

Figure 7 (cont.): c) Angular dependence of rescattered Ξ^-, d) Angular dependence of rescattered proton.

Also simulated were the angular dependencies of the decay vertices. These can be found in Appendix 3. The simulation of these reactions provide a visualisation of the decay event and can hypothetically be compared to the path length plot which takes particle decay into account. However, their main purpose is for later use in the acceptance measurements, which highlights the frequency of detection of the simulated particles.

3.1.3 Path Length and Decay

Figure 8 displays the decay impact on the trajectory of travelling particles. The graph on the left is the complete path length of a travelling Ξ^- particle. It is the composite of the calculations of the length in the (x,y) plane and in the ($\bar{y}$,z) plane to represent the three-dimensionality of the length, as discussed in Section 2.2.2.

The graph on the right is the simulated path length when the hyperon decay is accounted for. If the cascade is produced at a small angle, it is more likely that it travels the full length of the target provided it does not decay. When produced at a larger angle, the particle seems to exit the target very quickly after entering. Other than this, it is implied that the particle decays before travelling a sufficient distance. For example, in the left graph, it can be seen that there is a concentrated area of decay, the yellow and red regions, between 27 to 39 degrees at only about 3 centimetres into the target. This is a stark contrast to the particles produced up to about 10 degrees, travelling through the whole length of the target as depicted by the dark blue region.

Comparison of the two graphs in Figure 8 emphasises the impact that the Ξ^- hyperon decay has on the path length. Panel a) shows that there are more hyperons that travel the full length of the target, shown by the increased density of the dark blue region between 0 and 15 degrees. They are also shown to have a short path length between the same ranges as in panel b), but by about 5 cm longer than the decay influenced length, as depicted by the shift in concentration.

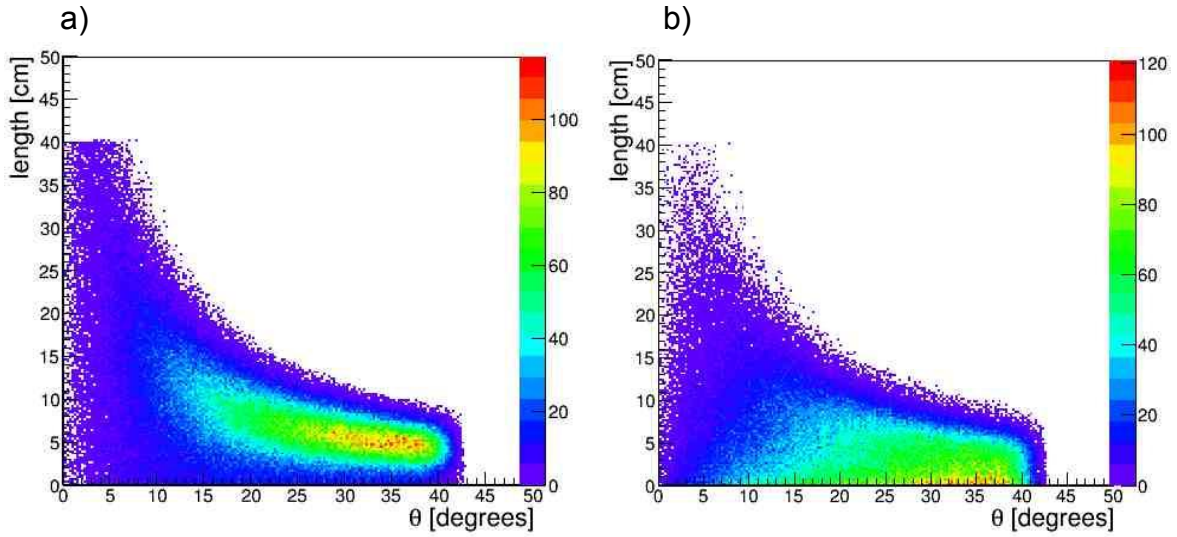

Figure 8: Path length. a) A plot of the path length of Ξ^-. b) A plot of the angle at which Ξ^- decays at which length on average.

Figure 9a) shows the momentum plotted with respect to the path length. It shows that the particle interaction has higher momentums at shorter lengths of the target. Further into the target the momentum decreases exponentially. This is due to the nature of the decay of Ξ^-, as shown in Figure 9b). The simulated path length that Ξ^- travels prior to decaying is to be expected due to its short lifetime of 0.1639 nanoseconds [5].

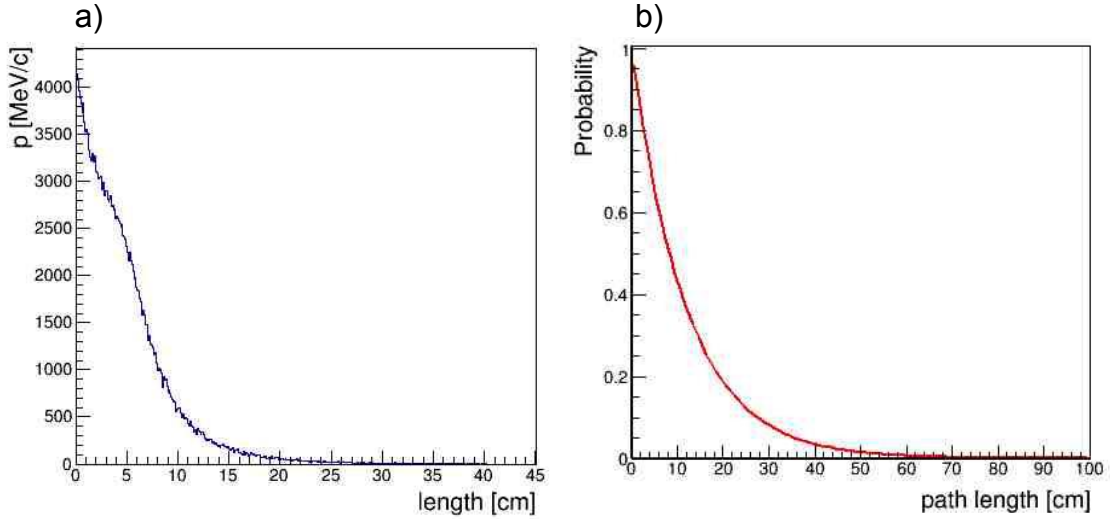

Figure 9: The exponential decay of Ξ^-. a) A plot of the momentum at which Ξ^- decays at which length on average. b) The exponential function of Ξ^- decay. Derivation of plot found in [A2.3].

3.1.4 Acceptances and Flux

The “acceptance” of a particle, in this instance the particles produced by the decay of the cascade, is the percentage of particles detected at a given parameter. This is a representation of the probability of the interaction having occurred at said parameter. It is not to be confused with the probability that a particle is detected - the data shows a particle that is detected, whilst also showing the probability of the interaction

happening within the parameters it was detected in based on the density of detection when compared with other regions. This is made visible in the histograms, with the same density scale as previous two-dimensional histograms.

The acceptance of the K_L momentum is used to calculate the number of detected events. The acceptances are shown below in Figure 10. The two histograms used to create Figure 10b) are shown superimposed on one another in panel a). These are both momentum acceptance components. Both graphs have a peak at 4 GeV/c. The smaller graph is the momentum acceptance of the beam when just accounting for random sampling. The larger one is taking into consideration the limitations of the detector, such as the efficiency and the spacing between the target and detector panel. When dividing the smaller graph by the larger one, the height of the peaks at that point meet at a lower midpoint, which is how the graph on the right is formed. This also explains why Figure 10b) appears to be greater in value and taper off at around 8 GeV/c - the two constituent graphs have small values at 8 GeV/c without as large of a discrepancy between them as at 4 GeV/c.

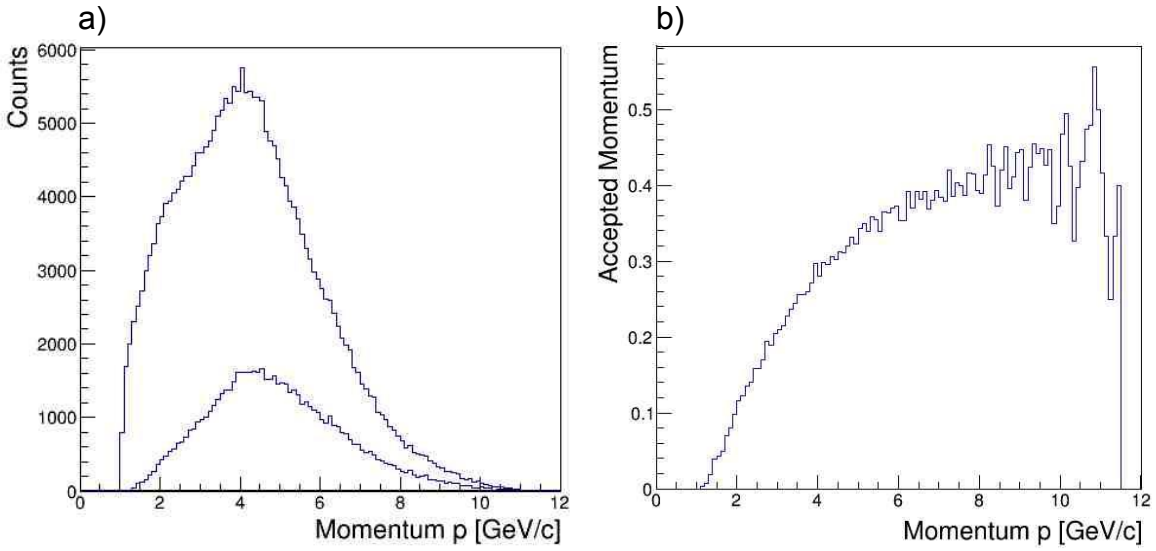

Figure 10: The acceptance of the K_L beam momentum. a) Constituent histograms of panel b). b) Result.

The histograms shown below in Figures 11 and 12 represent the flux of production events and scattering events respectively. Figure 11 takes into account the flux of the K_L particles by multiplying the histograms shown in Figures 4 and 5 respectively. This is what causes the apparent double hump. It has a peak at 2 GeV/c, decreases to a short plateau at roughly 4 GeV/c and then decreases from there. It is seen that there are no particles from the beam which produce hyperons with a momentum of higher than 12 GeV/c. The same concept applies for Figure 12, where the histograms in Figures 9 and 10 are multiplied.

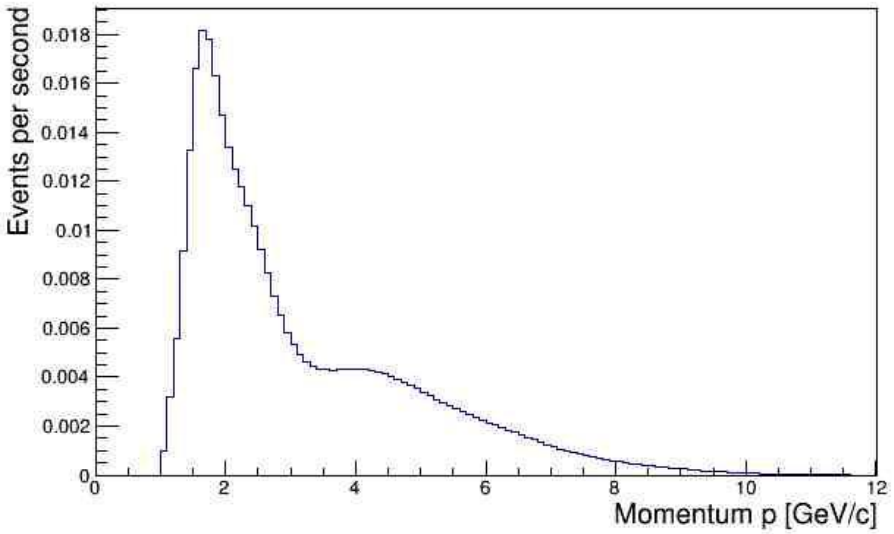

Figure 11: Momentum of the beam with respect to the flux of the produced hyperons.

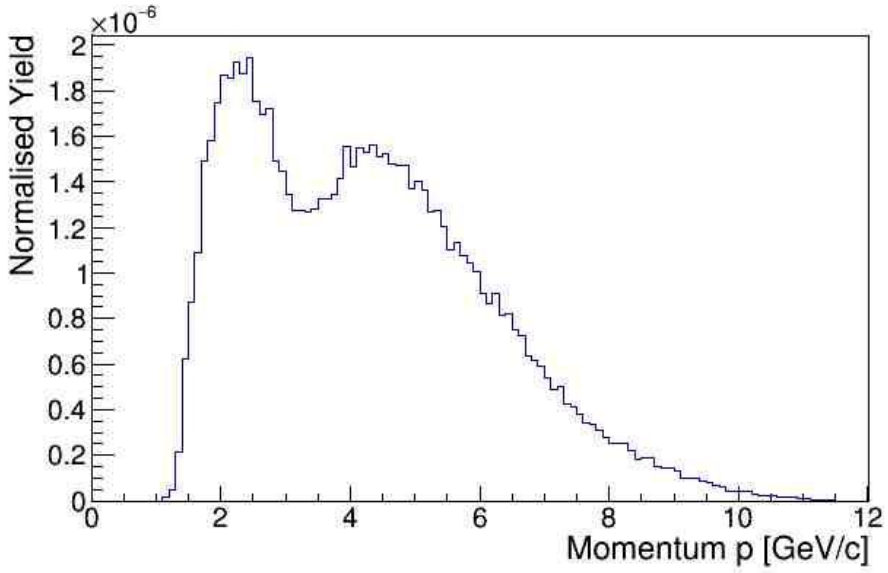

Figure 12: Yield per GeV/c of momentum of the Ξ^- hyperons.

The acceptance of each vertex of the interaction is required to compute the final number of detected scattering events. Integrating Equation 4 produces the total number of events for each production, scattering, and detection flux, displayed in Table 1.

Number of produced Ξ^- hyperons over 100 days	3.07636×10^6
Predicted number of scattered Ξ^- hyperons over 100 days	3718.01
Number of detected scattered Ξ^- hyperons over 100 days	692.403

Table 1: Results of the completed simulation on the first iteration for 250,000 events.

The latter two entries of Table 1 are subject to the simulation being run consecutively. As it is iterated, these two values decrease. All computed acceptance histograms can be seen in Appendix 5. The empty data range seen on some of the plots is due to the KLF detector's operating parameters.

3.2 Discussion

The complete particle interaction was simulated to run over the span of 100 days in accordance with the experiment proposed for JLab. In order to simulate this timespan, the macro was set to simulate 250,000 events and integrate in seconds, between 0 to 8,460,000, in order to maintain standard units [A1.2]. Over this simulated time period, the predicted number of detected scattering events of cascades being roughly 692 from over 3 million having been produced seems small. Since Ξ^- decays too quickly, it is likely that less scattered particles will be detected - just under one-fifth of particles were detected out of all predicted to scatter [A2.4]. Despite the fact, this is still a sufficient number to extract data points from, since it is an improvement from the current statistics of 3 measured events available for this interaction. Building from this initial point is therefore feasible.

On the first iteration of the macro, the error in the detector acceptance can be calculated using the values in Table 1 in order to get an uncertainty of ±0.01 (~1%) [A2.5]. This naturally reduces itself, however, as the macro is run repeatedly. The uncertainty in the scattered particle magnitude was computed as $\pm 2 \times 10^{-5}$ using the same method as for the detected magnitude, which can be considered negligible. The reason the uncertainty is so small is likely due to the number of events simulated being high. If the number of events were increased above 250,000, the uncertainty would likely decrease further.

In essence, the data obtained in this simulation project cannot be as entirely realistic as possible because of several assumptions that have been made. For example, due to an absence of data the cross sectional data for a different production event was used in place of the proposed interaction event. There is a subsequent possibility that doing this yields a different result to reality, and in practice, it would not be known until that data was actually measured. For the purpose of the simulation, assuming that the statistics of this interaction are similar shall have to suffice. There are no other similar interactions with masses as comparable to the proposed interactions. Should the production cross section be smaller than the assumed value, the number of produced events would probably be much smaller, and similarly if the cross section was larger. This would then lead to a decrease in the predicted and detected scattering events. Nonetheless, this simply means we may assume that the relationship between cross section and flux of particles is proportional. It is therefore permitted in this instance that this assumption is made, so long as it is kept in mind and modified in future experiments once a more reliable measurement is gathered.

4. Conclusion

The long-term motivation for expanding our knowledge on hyperons and their nucleon interactions is to develop a more intricate understanding of the workings of our universe. There are indications that particles with strangeness, such as

hyperons, have different transition temperatures during hadronization from particles without this flavour [15], which alludes to the question of whether strange quarks will populate excited states more frequently in particular resonances [8]. Studying and recording measurements of these components of hyperonic behaviour are ultimately the link to the future understanding of the process of hadronization, particularly within neutron stars. As displayed previously in Figure 1, the existence of hyperons in a neutron star impacts the EoS and the measured mass of the star. This is why the Ξ^- + p scattering interaction, amongst other hyperon-nucleon processes, is a key point of interest for future research.

The original aims of the project were to create a functional macro that simulates the interaction defined in Equations 1 and 2, and determine the feasibility of running the experiment at JLab based on whether the results of the simulation predict a satisfactory number of detected scattering events. The key finding that the 692 scattered hyperons were detected with an acceptance uncertainty of roughly 1% and decreasing with every consecutive run is in line with the expected systematic uncertainty of the GlueX detector of less than 3% [8,16].

In regards to possible improvements to the experiment, it would be interesting to consider how the detector can be modified, and any incentives that motivate an improvement. In theory, the acceptance can be improved by changing the width of the gaps between each component of the detector. This would lead to the detection of more scattered particles, a higher proportion than the predicted ~19%. Another way of improving the experiment would be via the target. The deuterium target is to be shielded by a lead shielding, where a tungsten-lead mix would contain radiation and heat dissipation more effectively to conserve energy [7]. However, the factor preventing both of these modifications is simply cost. The high cost of the experiment at JLab is why a feasibility study is required, as there is futility in running an experiment to get minimal results out of it.

The final conclusion on feasibility is that the simulation meets the minimum requirements for the experiment to produce appropriate results. Because there is little-to-no data available for neutral kaons scattering on a neutron target, this is an excellent opportunity to commence a first-of-its-kind experiment, using a uniquely designed beam with K_L fluxes three magnitudes higher than previously achieved. The measurements of hyperon-nucleon interactions by large detector facilities such as KLF will lead to data that provides roughly 40 times the available statistics on hyperonic photoproduction [8]. This will shed further light on the hyperon puzzle, accomplishing a detailed understanding of the topic. Hence, the feasibility of running this experiment with a beamtime of 100 days is high, and should be concretely considered.

Appendices

APPENDIX 1: Code

1.1 C++ Macro

The full C++ macro used for the production of the simulated data in this project can be accessed at https://github.com/mayajovanovic/bscproject.

1.2 Event Number Calculations

```
142 h_beamflux->Multiply(h24p,hKPXi1);
143 h_beamflux->Scale((6.022E-9/2.014)*0.1624*targetlength);
144 cout<<"Total number of Xi produced over 100 days: "<<
    h_beam_momentum->Integral()*100*24*60*60 << endl;
```

```
317 h_scattered_xi=(TH1F*)h_beamflux->Clone("h_scattered_xi"
318 );
    h_scattered_xi->Scale((h_filledpathlength->GetMean())*(6
    .022E-4/2.014)*0.1624*5.25);
319 cout<<"Total number of predicted scattered Xi over 100
    days: "<< h_scattered_xi->Integral()*100*24*60*60 <<
    endl;
```

```
322 h_detected_xi->Multiply(h_beamflux,h_kl_momentumacceptan
    ce);
323 h_detected_xi->Scale((h_filledpathlength->GetMean())*(6.
    022E-4/2.014)*0.1624*5.25);
324 cout<<"Total number of detected scattered Xi over 100
    days: "<< h_xi_scatteringevents->Integral()*100*24*60*60
    << endl;
```

The above lines print the results shown in Table 1 respectively.

APPENDIX 2: Calculations

2.1 Path length calculations

Let the distance from the origin of the axes to the point of entry of the particle, (x,y,z), be denoted as r_{vertex}. The value for $\phi_{particle}$ is obtained via the ROOT libraries, but can be considered generally in this derivation.

The distance r_{vertex} is in essence is simply equal to $\sqrt{x^2 + y^2}$, since the z-axis is not taken into account. The angle denoted α is calculated by addition of the angles denoted 180 - ϕ_{vertex} and $\phi_{particle}$. ϕ_{vertex} is the angle between the x-axis and r_{vertex}, easily calculated using $tan^{-1}(\frac{y}{x})$. $\phi_{particle}$ is the angle the particle scatters at to the plane parallel to the x axis.

The radius of the target, R, can be expressed in terms of the other components as:

$$R = r_{vertex}^2 + L^2 - 2Lr_{vertex}cos(\alpha)$$

This rearranges to:

$$L^2 - (2r_{vertex}cos(\alpha))L + r_{vertex}^2 - R^2 = 0$$

Solving for L is done via the quadratic equation:

$$L = r_{vertex}cos(\alpha) \pm \sqrt{r_{vertex}^2 cos^2(a) + R^2 - r_{vertex}^2}$$

The z vertex of the exit position (z') is calculated as $z' = L' + z$, where z is the z-vertex of the beam entry.

If the particle were to exit from the top or bottom of the cylindrical target, $L' = \frac{L}{tan(\theta)}$ and $L' = L_t - z$ if z' is either larger than the target length, or smaller than 0.

2.2 Threshold momentum of K_L beam

Momentum is conserved in all particle interactions. In terms of four-vectors, $\hat{p}$, the initial vertex of the interaction in the lab frame of reference is described like so:

$$\left((p_x, p_y, p_z, m_{Kl}) + (p_x, p_y, p_z, m_n)\right)^2 = \left((p_x, p_y, p_z, m_{K+}) + (p_x, p_y, p_z, m_{\Xi-})\right)^2$$

The square of a four-vector is simply equal to the mass squared, since for all spatial components of $\hat{p}$ apart from the beam (which we don't consider, as we want to find the minimum value), the initial momentum is 0.
Expanding the above,

$$m_{Kl}^2 + m_n^2 + 2E_{Kl}m_n = m_{K+}^2 + m_{\Xi-}^2 + 2m_{K+}m_{\Xi-}$$

The energy value E_{Kl} is the total energy of the beam. This is also given by $\sqrt{p_{Kl}^2 + m_{Kl}^2}$. The goal is to rearrange the equation to solve for E_{Kl}, and then using the found value, rearrange the definition of E_{Kl} to determine p_{Kl}, which is the threshold momentum of the beam for it to have this energy.

The masses of all included particles are known in terms of GeV/c, and can be found via the Particle Data Group [5]. Solving for E_{Kl} gives:

$$E_{Kl} = 1.15384 \text{ GeV/c} = \sqrt{p_{Kl}^2 + m_{Kl}^2}$$

$$\Rightarrow p_{Kl} = \sqrt{1.15384^2 - m_{Kl}^2} = 1.04 \text{ GeV/c}$$

2.3 Exponential decay

$$y = exp\left(\frac{-x}{[0]*[1]*30*0.1639}\right)$$

In the above equation, the x variable represents the path length. The parameters [0] and [1] are the decay parameters of Ξ^-, using randomly sampled beta and gamma decay functions from the ROOT libraries (see Appendix 1). The number 30 is the speed of light in centimetres per nanosecond, and 0.1639 is the mean lifetime of Ξ^- in nanoseconds, thus preserving unit magnitude and keeping the calculations in terms of centimetres as in the whole macro. It is therefore as expected that the graphs in Figures 8 and 9 follow the same decay curve as the general decay of Ξ^-.

2.4 Percentage of events detected from scattering

$\frac{692.403}{3718.01} = 0.186$, which is just under 20%.

2.5 Uncertainty in the acceptance

The uncertainty is calculated using propagation of errors. The formula to use to calculate the error in this instance is

$$\sigma_f^2 = f^2 \cdot \left[\left(\frac{\sigma_A}{A}\right)^2 + \left(\frac{\sigma_B}{B}\right)^2 - 2\frac{\sigma_{AB}}{AB}\right]$$

where $f = \frac{A}{B}$, $A = Yield_{detected}$, $B = Yield_{scattered}$, $\sigma_A = \sqrt{A}$, $\sigma_B = \sqrt{B}$

Using the values displayed in Table 1 and calculating for σ_f we obtain the following:

$$\sigma_f = \frac{692.403}{3718.01}\sqrt{\left[\left(\frac{\sqrt{692.403}}{692.403}\right)^2 + \left(\frac{\sqrt{3718.01}}{3718.01}\right)^2 - 2\frac{\sigma_{AB}}{AB}\right]}$$

$- 2\frac{\sigma_{AB}}{AB} = 0$ because we can neglect the errors in cross section and luminosity.

$$\sigma_f = \frac{692.403}{3718.01}\sqrt{\left[\left(\frac{\sqrt{692.403}}{692.403}\right)^2 + \left(\frac{\sqrt{3718.01}}{3718.01}\right)^2\right]} = 7.7 \times 10^{-3}$$
$$= 0.0077 \approx 0.01$$

Hence the uncertainty in the acceptance on the first iteration is $\pm\ 0.01$ to two decimal points.

APPENDIX 3: Angular Dependence Histograms

For the angular dependence histograms not included in Section 3.1.2

Decayed particle scattering

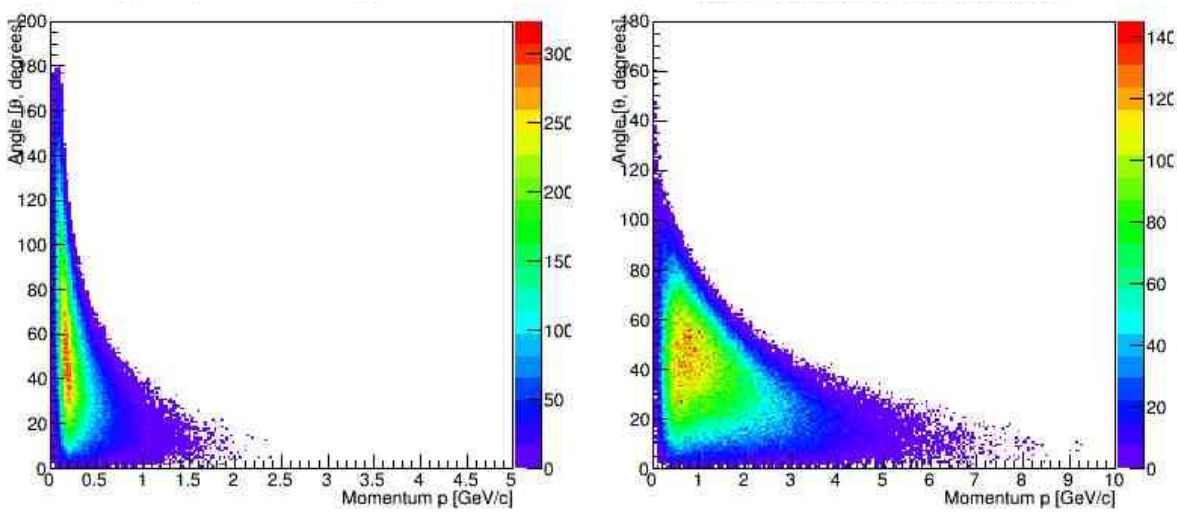

a) Ξ^- produced π^-
b) Ξ^- produced Λ^0

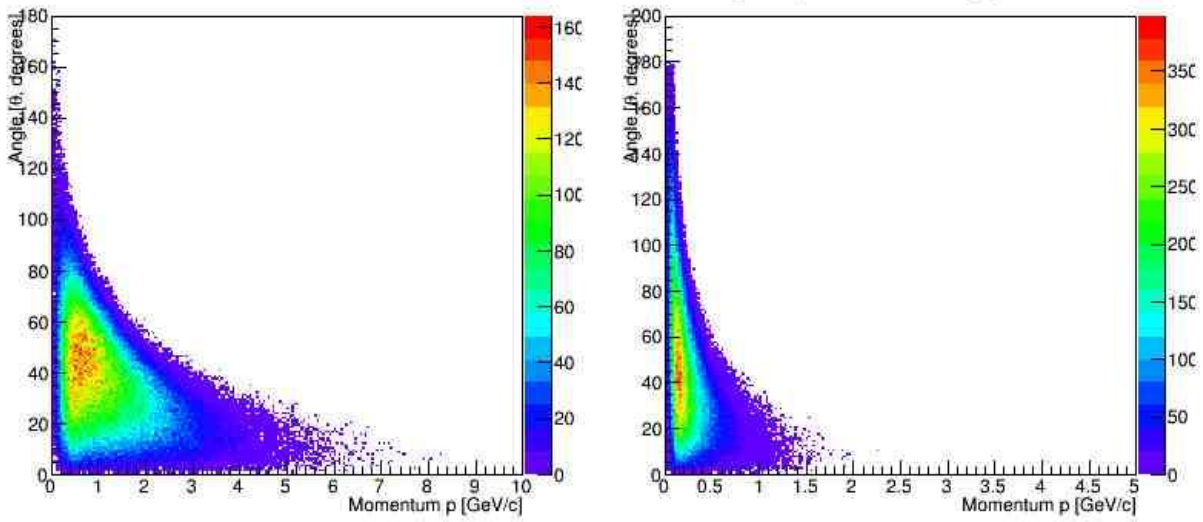

a) Λ^0 produced proton
b) Λ^0 produced π^-

APPENDIX 4: Path Length Histograms

For the histograms not included in Section 3.1.3

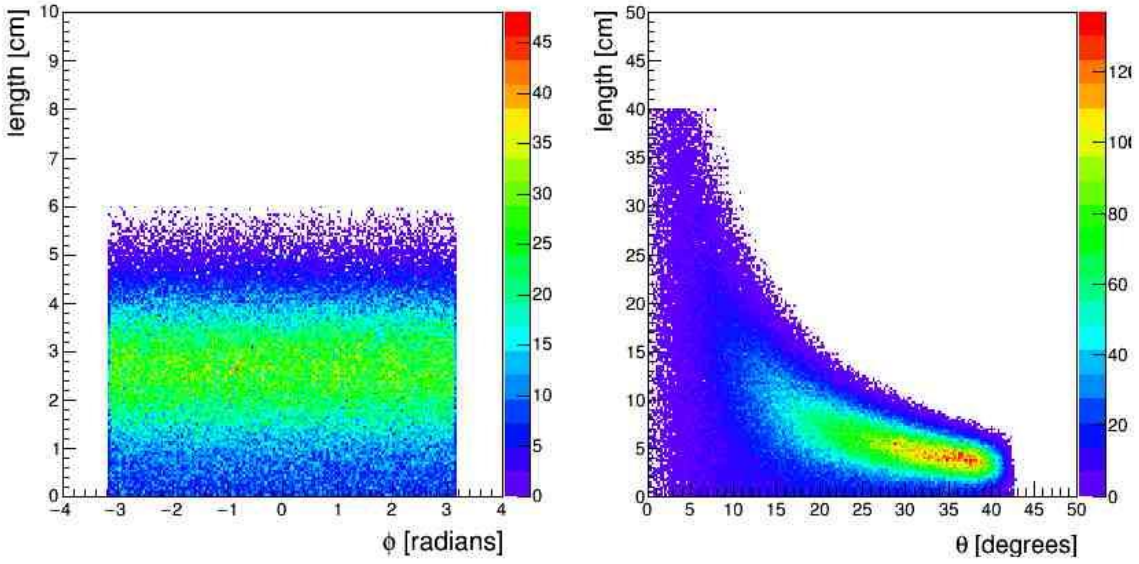

a) The angle at which the hyperon scatters in the (x,y) plane.
b) The angle at which the hyperon scatters in the (ȳ,z) plane.

APPENDIX 5: Acceptance Histograms

For the acceptances not included in Section 3.1.4

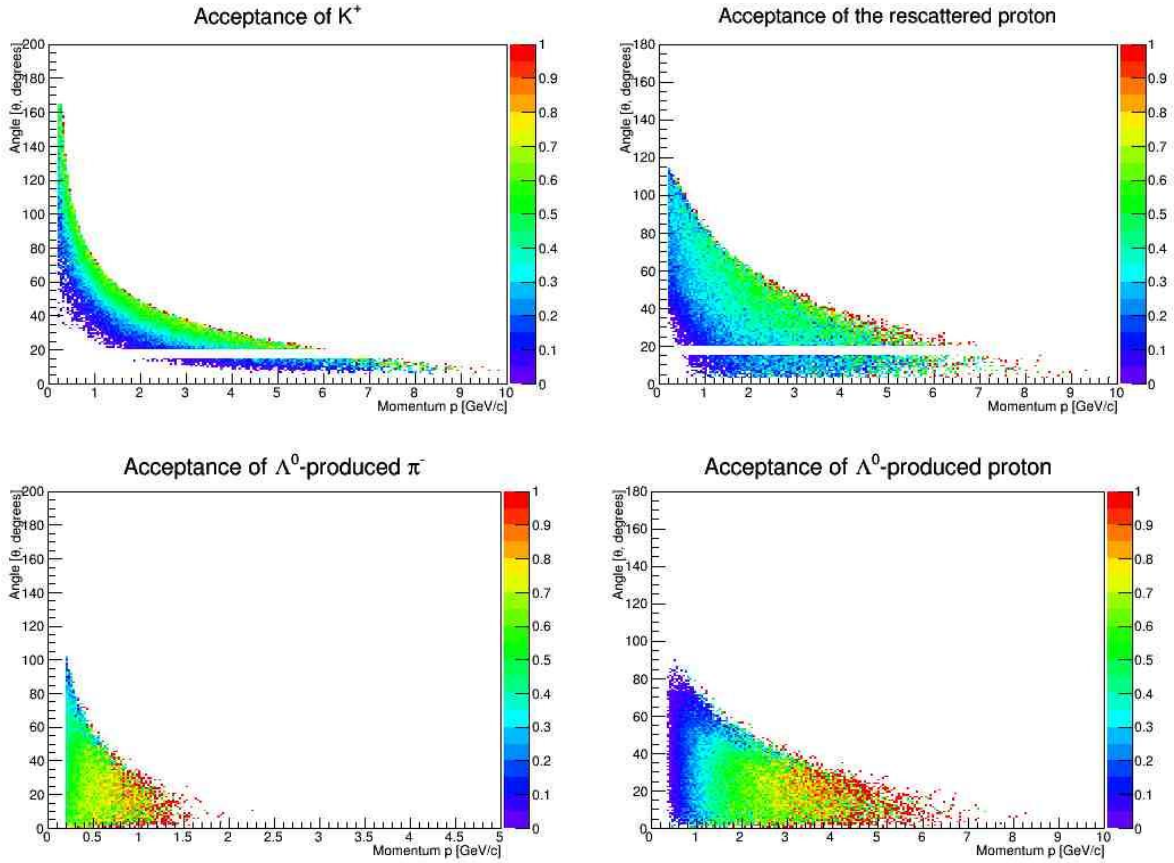

Appendix 5 cont.

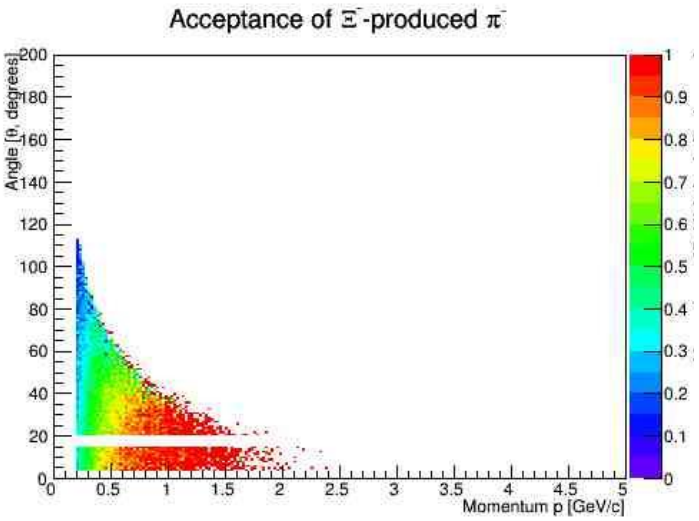

References

[1] J. Schaffner-Bielich, M. Hanauske, H. Stöcker, and W. Greiner, *Phase Transition to Hyperon Matter in Neutron Stars*, Physical Review Letters **89**, (2002).

[2] I. Bombaci, *The Hyperon Puzzle in Neutron Stars*, Nuclear Physics News **31**, 17 (2021).

[3] I. Vidaña, *Hyperons in Neutron Stars*, Journal of Physics: Conference Series **668**, (2016).

[4] R. A. Hulse and J. H. Taylor, *Discovery of a pulsar in a binary system*, Astrophys. J. Lett **195**, L51 (1975).

[5] P. A. Zyla et al (Particle Data Group), *Review of Particle Physics*, Progress of Theoretical and Experimental Physics **2020**, (2020).

[6] R. Abbott, T. D. Abbott et al, *Observation of Gravitational Waves from Two Neutron Star–Black Hole Coalescences*, The Astrophysical Journal Letters **915**, (2021).

[7] A. Ali, F. Barbosa, et al, *The GLUEX DIRC Program*, Journal of Instrumentation **15**, (2020).

[9] M. Amaryan, M. Bashkanov et al, *Strange Hadron Spectroscopy with Secondary KL Beam in Hall D*, KLF Collaboration (2021).

[9] A. Aleksejevs, S. Barkanova et al, *An Initial Study of Mesons and Baryons Containing Strange Quarks with GlueX*, GlueX Collaboration (2013).

[10] M. Bashkanov, N. Zachariou et al, *KLF Analysis Report: Hyperon Spectroscopy Simulation Studies*, (2021).

[11] Webpage by CERN Organisation, *About ROOT*, https://root.cern/about/.

[12] Webpage by CERN Organisation, *ROOT: Class List*, https://root.cern/doc/master/annotated.html.

[13] W. Herr and B. Muratori, *Concept of Luminosity* (CERN, 2006).

[14] P. Capiluppi, G. Giacomelli et al, *A COMPILATION of $K^0_L p$ CROSS SECTIONS*, IFUB 81-25 (Bologna Univ. Ist. Fís, Bologna, 1981).

[15] R. Bellwied, S. Borsanyi, et al, *Is there a flavor hierarchy in the deconfinement transition of QCD?*, Phys. Rev. Lett. **111**, 202302 (2013).

[16] The GlueX Collaboration, H. Al Ghoul et al, *Measurement of the beam asymmetry Σ for π^0 and η photoproduction on the proton at E_γ = 9 GeV*, Phys. Rev. C **95**, no. 4, 042201 (2017)